THE OFFICIAL MAGAZINE OF THE OCEANOGRAPHY SOCIETY

Oceanography

CITATION

Flores-Melo, X., I.R. Schloss, C. Chavanne, G.O. Almandoz, M. Latorre, and G.A. Ferreyra. 2018. Phytoplankton ecology during a spring-neap tidal cycle in the southern tidal front of San Jorge Gulf, Patagonia. *Oceanography* 31(4):70–80, https://doi.org/10.5670/oceanog.2018.412.

DOI

https://doi.org/10.5670/oceanog.2018.412

Phytoplankton Ecology During a Spring-Neap Tidal Cycle in the Southern Tidal Front of San Jorge Gulf, Patagonia

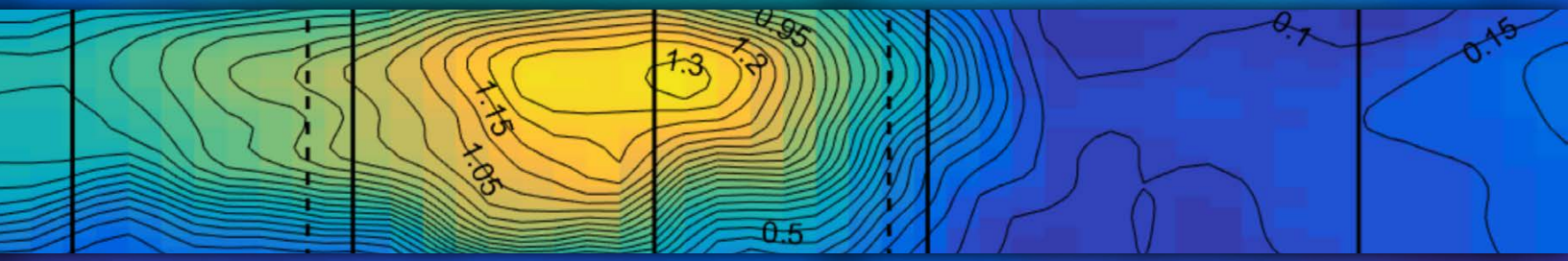

By Ximena Flores-Melo, Irene R. Schloss, Cédric Chavanne, Gastón O. Almandoz, Maité Latorre, and Gustavo A. Ferreyra

ABSTRACT. Tidal fronts are interfaces that separate stratified from mixed waters. The stratified surface zone of a front has lower inorganic nutrient concentrations than the mixed side, and thus, phytoplankton assemblages are expected to differ from one side of the front to the other. Here, we characterize the physics, nutrient dynamics, and biology of the southern front in San Jorge Gulf (SJG), Argentina, during a spring-neap tidal cycle. Baroclinic instabilities influence the shape and position of the front and presumably play an important role in the horizontal transport across the front. The highest phytoplankton biomass concentrations were found in the waters of the stratified side of the front during neap tide, with picophytoplankton, cyanobacteria, and nanophytoplankton being the main contributors to the total autotrophic biomass. Bacteria contribute the most to heterotrophic biomass. In contrast, during spring tide, the carbon contribution of microphytoplankton was higher than during neap tide. In the mixed side, cells photoacclimate to optimum light conditions, suggesting that cells near the surface, which are probably photoinhibited, and cells below the euphotic zone, which are light-limited, are quickly advected by turbulent vertical motions to depths with optimal irradiance conditions.

INTRODUCTION

Marine fronts are transitional areas between two water masses with different properties (Acha et al., 2015), and they exhibit strong horizontal density gradients. In temperate coastal regions, where the water column becomes stratified in summer, tidal currents can provide the turbulent energy required to break stratification (Landeira et al., 2014). Because the strength of tidal-induced mixing decreases from the bottom to the surface, tidal energy has to be stronger to erode the pycnocline in deeper waters, while the shallowest coastal waters remain mixed throughout the entire tidal cycle, even during minimal turbulent energy periods (Loder and Platt, 1985). In a special case, a tidal front separates stratified deep waters from mixed shallow waters, and its position depends on tidal energy as well as bottom depth (Simpson and Hunter, 1974).

When the pycnocline of the stratified side of the front is shallower than the euphotic depth, irradiance conditions for photosynthetic organisms are optimal in the upper layer. However, the same pycnocline restricts the availability of inorganic nutrients, which usually occur in higher concentrations in deeper waters. In contrast, on the well-mixed side, mixing brings inorganic nutrients from deeper waters to the euphotic layer and also transports phytoplankton cells to poorly lit depths (Pingree et al., 1978). Nevertheless, the horizontal advection of water and front displacements favor the input of nutrients to surface layers (Landeira et al., 2014).

Maximum chlorophyll-*a* (Chl-*a*) concentrations (a proxy for phytoplankton biomass) are usually found in the upper mixed layer on the stratified side of tidal fronts (Landeira et al., 2014), and decrease away from the frontal interface toward offshore waters (Franks, 1992). The environmental variations in the frontal area, related to upper mixed layer depth, euphotic depth, and nutrient supply, enhance primary production and allow the development of different phytoplankton assemblages (Margalef, 1978). Glibert (2016), revisiting Margalef's mandala on interactions among dissolved inorganic nutrients, turbulence, and light levels, suggests that it would be possible to predict the dominant phytoplankton groups along environmental frontal gradients. Diatoms dominate where turbulent energy renders dissolved inorganic nutrients available in the euphotic layer so that the N:P ratio is expected to approach the Redfield ratio (Glibert, 2016). Additionally, microphytoplankton groups (>20 μm) such as dinoflagellates and other flagellates dominate the stratified side of the front. However, the smallest groups, such as pico- and nanoeukariotes and cyanobacteria (<20 μm), will be more important than microphytoplankton if the stratified side has a lower N:P ratio.

The organic matter produced by phytoplankton photosynthesis constitutes the base of marine trophic food webs. It is rich in proteins, carbohydrates, and lipids (i.e., of high nutritional value for higher trophic levels; Copin-Montegut and Copin-Montegut, 1983). A proxy for the nutritional quality of organic matter is the particulate carbon to nitrogen ratio (C:N ratio; Townsend and Thomas, 2002), which is low (i.e., high protein content) when micro- and nanoplankton biomass increase (Townsend and Thomas, 2002). This, in turn, relates to the physiological status of cells that is affected by both light conditions and nutrient concentrations, and can be evaluated by their fluorescence response (Maxwell and Johnson, 2000; Moore et al., 2006).

San Jorge Gulf (SJG) is a semi-enclosed basin where the center reaches a maximum depth of 100 m. The area is characterized by strong winds whose summer mean speeds are ~8–10 m s^{-1} (Barros, 1983). A thermocline forms in spring and starts to disappear in late autumn (Fernández et al., 2008). During summer, the thermocline (here, temperature is the main factor contributing to vertical stratification) reaches 30–50 m depth (Cucchi-Colleoni and Carreto, 2001). In the southeast SJG, bathymetric features rise to as much as 60 m above the seafloor (Glembocki, et al., 2015) and are associated with a tidal front, as evidenced by a sharp spatial temperature gradient in surface waters during spring and summer (Louge et al., 2004). Tidal energy here is among the strongest in the world, with currents reaching 3.5 m s^{-1} in a clockwise rotation in the southern gulf (Tonini et al., 2006). This region also exhibits the greatest tidal energy dissipation by bottom friction of all of Argentinean Patagonia. The semidiurnal tidal (M2) constituent explains more than 80% of tidal kinetic energy variance in the area (Rivas, 1997). This seasonal tidal front has been identified in satellite images (Fernández et al., 2005; Glembocki et al., 2015), as well as through the estimation of the Simpson-Hunter parameter (Glorioso and Flather, 1995) and modeling of tidal circulation and winds (Palma et al., 2004).

The southern front area exhibits high Chl-*a* concentrations during austral summer (Rivas, 2006), allowing the development of a diverse and abundant benthic community (Fernández et al., 2005). In addition, it is an area of significant larval retention for the Argentinean red shrimp *Pleoticus muelleri* (Glembocki et al., 2015).

Most investigations of tidal fronts and nutrient distribution focus on vertical fluxes, without considering the role of horizontal fluxes. Despite the importance of fronts' spatial and temporal variabilities, which modulate nutrient dynamics and key phytoplankton parameters such as assemblage compositions, carbon accumulations, and photosynthetic responses, knowledge of these processes in the southern SJG is still very limited.

In this context, the main goals of this

investigation are to study (1) the temporal variability of the southern SJG front position during a spring-neap tidal cycle, (2) how physical variability affects nutrient availability, and (3) how the phytoplankton community responds to physical and nutrient concentration variations in the front, considering phytoplankton biomass accumulation, cells' physiological state, and the relationship with microheterotrophs.

METHODOLOGY

Characterizing the Front

The frontal area in the southeastern SJG was studied from February 5 to February 9, 2014, during a cruise aboard R/V *Coriolis II* (Figure 1). The approximate position of the front was first identified in satellite images of sea surface temperature (SST; Figure 2; see methods in the online supplementary material). Eighteen cross-frontal transects were then conducted to characterize the front, and 10 CTD-rosette stations sampled biological, physical, and chemical variables. On February 5, under spring tide conditions, the first six transects and five discrete stations were sampled over the southern transect. The other six transects and five stations over the southern transect were sampled from February 8 to February 9 during the beginning of neap tide conditions. Prior to the six transects conducted during neap tide, six overlapping transects were run over 12 hours in order to characterize the frontal excursion caused by the M2 constituent displacement.

Continuous water column data were recorded with the undulating, remotely operated towed vehicle (ROTV) ScanFish II, equipped with temperature/salinity (SBE 49 FastCAT) and fluorescence (WET Labs model ECO-FL-NTU) sensors. These sensors were calibrated by Sea-Bird Scientific before and after the cruise. Six 30 km long transects across the front were tracked during the spring and neap tides, spaced approximately 3 km from each other, covering a total frontal region of 450 km^2 (Figure 1). Horizontal current speed and direction were measured with a hull-mounted 150 kHz acoustic Doppler current profiler (ADCP), and bottom topography data were collected with a hull-mounted Simrad EK-60 echosounder. The surface frontal positions were identified by calculating the maximum along-track density gradient, which coincided with the 24.9 kg m^{-3} isopycnal at 5 m depth. Frontal positions were later relocated for tidal advection using measured currents and a reference point along the transect corresponding to the passage of the Moderate Resolution Imaging Spectroradiometer (MODIS) satellite. Currents were depth-averaged and projected on the transects' direction.

Vertical Profile Characterization

Water-column samples were collected at discrete stations using 12 L Niskin bottles installed on a rosette. Stations during

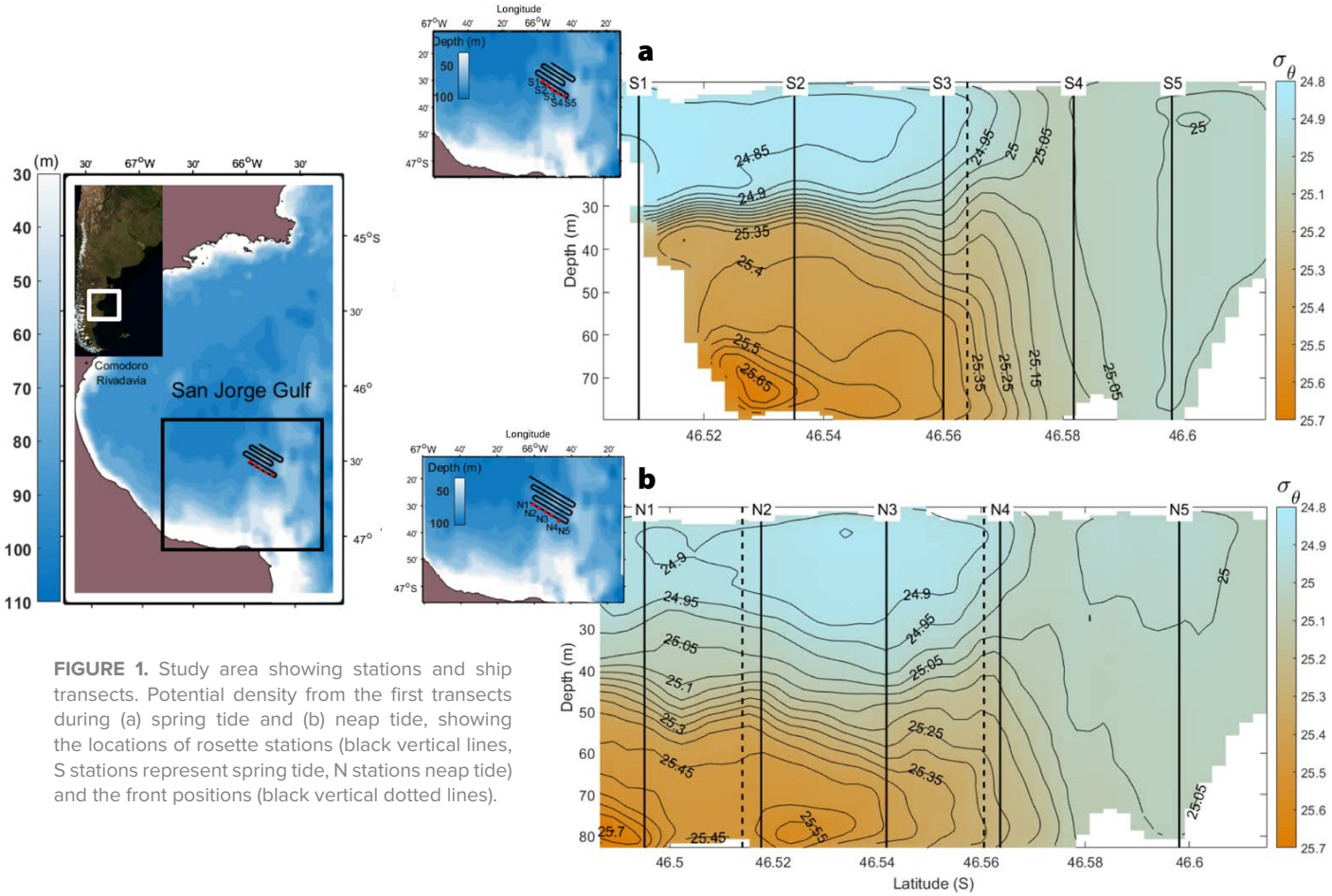

FIGURE 1. Study area showing stations and ship transects. Potential density from the first transects during (a) spring tide and (b) neap tide, showing the locations of rosette stations (black vertical lines, S stations represent spring tide, N stations neap tide) and the front positions (black vertical dotted lines).

each tidal period were located ~5 km from each other across the frontal zone, ensuring that both sides of the front were sampled. Stratification strength was estimated with vertical temperature (°C), conductivity (S m^{-1}), and depth (m) profiles collected using an SBE 911plus CTD, and calculating the Brunt-Väisälä frequency N^2 (Figure 3). Photosynthetically active radiation (PAR) was measured with a LI-COR Biospherial probe, and euphotic depth or Z_{eu} (the depth of 1% surface irradiance; Kirk, 1994) was estimated for those stations sampled during daytime (i.e., before 19:00 hr—stations S3, N1, N3).

Water was sampled for nitrate, nitrite, phosphate, and silicate at three out of the five stations for each tidal period (stations S3, S5, S1 for spring tide and stations N1, N3, N5 for neap tide) at two depths above the pycnocline (subsurface and Chl-*a* maximum; see methods in supplementary material).

Microbial Community

Discrete water samples (100 ml) were collected at Chl-*a* maximum depth from the same six stations (S3, S5, S1, N1, N3, and N5). They were fixed with acidic Lugol (final concentration 4%) and stored at 4°C in the dark for phytoplankton composition, abundance, and biomass (as phytoplankton carbon) studies. Methods are presented in supplementary material.

The physiological state of photosynthetic cells, the maximum photochemical quantum efficiency of photosystem II (***F***v/***F***m), and the connectivity parameter ***p*** were measured with a fast repetition rate fluorometer (Chelsea Instruments, UK; see methods in the supplementary material).

RESULTS

In this study, we focus on the surface expression of the southeastern front. It is the most relevant for phytoplankton, given its relationship with key variables such as the relative depths of the euphotic zone and the pycnocline, as well as nutrient availability (Figure 1).

The shape of the density structure at the front differed between spring and neap tides. During the spring tide (Figure 1a), the transition from the mixed to the stratified side was easily recognizable, varying in density from 46.58°S to 46.55°S ($\Delta\rho$ = 0.2 kg m^{-3}) at the surface. In contrast, during neap tide (Figure 1b), the transition between the mixed and the stratified sides was less sharp and presented two frontal boundaries (vertical dotted lines). At one of these boundaries, density at the surface varied from 46.58°S to 46.55°S ($\Delta\rho$ = 0.1 kg m^{-3}), and in the other, density varied from 46.58°S to 46.52°S ($\Delta\rho$ = 0.05 kg m^{-3}). Furthermore, the frontal position moved ~4 km northward from spring to neap tide.

To analyze the double frontal expression during neap tide, front positions (red dots in Figure 2a) were plotted over the surface density averaged between 3 m and 10 m and bathymetry. The figure shows that both fronts have a semicircular shape; the western front follows the ~90 m isobath, while the eastern front follows a depth gradient, from ~65 m to 85 m. In addition, the northern front position develops in waters deeper than 90 m. The structure observed during spring tide is presented in the supplementary material.

We then plotted the frontal position over a sea surface temperature (SST) image (Figure 2b) acquired from the NASA ocean color web page (https://oceancolor.gsfc.nasa.gov/) only for neap tide, because cloud cover prevented us from obtaining a similar image for spring tide. Several surface meanders were evident as the horizontal water mass intrusion from 66.2°W to 65.9°W, and

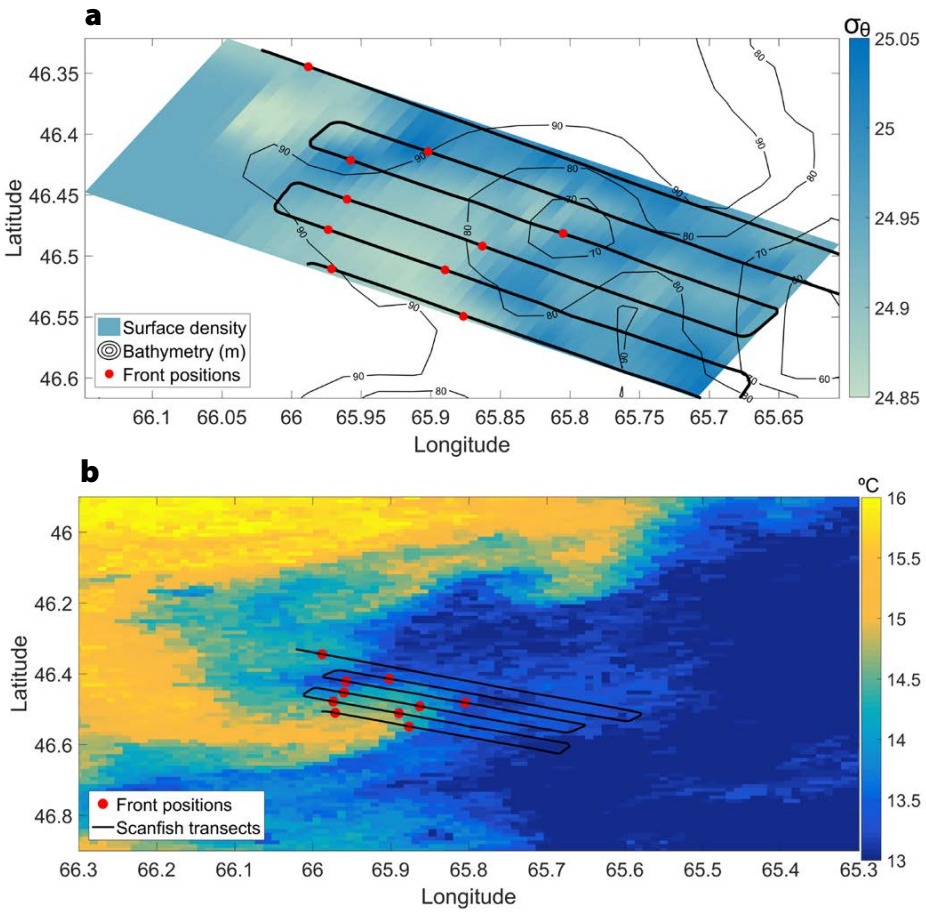

FIGURE 2. Frontal positions in the SJG during neap tide (red points). The colors represent average potential density between 3 m and 10 m depth in panel (a), and sea surface temperature (°C) derived from satellite sensors in panel (b). Data processing and figure construction were done using MATLAB (R2016a), and Gibbs Sea Water routines for MATLAB were used to treat the seawater thermodynamics data (McDougall and Barker, 2011).

between 46.6°S and 46.5°S. In a tongue-shaped structure, this intrusion carried warm (and therefore less dense) waters with temperatures around 15°–15.5°C that were easily distinguishable from the surrounding colder waters with temperatures around 13.5°–14°C. This structure suggests the presence of baroclinic instability, matching with the frontal positions estimated using the ROTV-collected density profiles.

Water Column Profiles

The profiles for the 10 discrete stations collected on February 5 and February 9 allowed us to further identify and characterize the vertical structures on both sides of the front and in the transitional zone. Stations S3 and N4 are the closest stations to the frontal interface (see Figure 1), so they can be considered part of the limit between the stratified and mixed sides of the front. The Brunt-Väisälä frequency N^2 (Figure 3) showed that station S3 had intermediate stratification conditions, while waters sampled at stations S1, N1, and N3 were well stratified, with maximum N^2 at around 40 m or slightly above that depth. This determines the depth of the upper mixed layer, which is the maximum depth to which phytoplankton cells are vertically transported from the surface.

Maximum Chl-*a* concentrations were found during neap tide at ~20 m depth at the stratified stations N1, N2, and N3, located between the two frontal boundaries (1–1.3 mg Chl-*a* m^{-3}). Stations S3, S4, S5, and N5 exhibited a well-mixed water column, without any marked pycnocline, and showed lower Chl-*a* concentrations (0.1–0.35 mg Chl-*a* m^{-3}). During both tidal periods, the highest Chl-*a* concentrations were found between the pycnocline and the surface, with maximum values around 10–25 m depth.

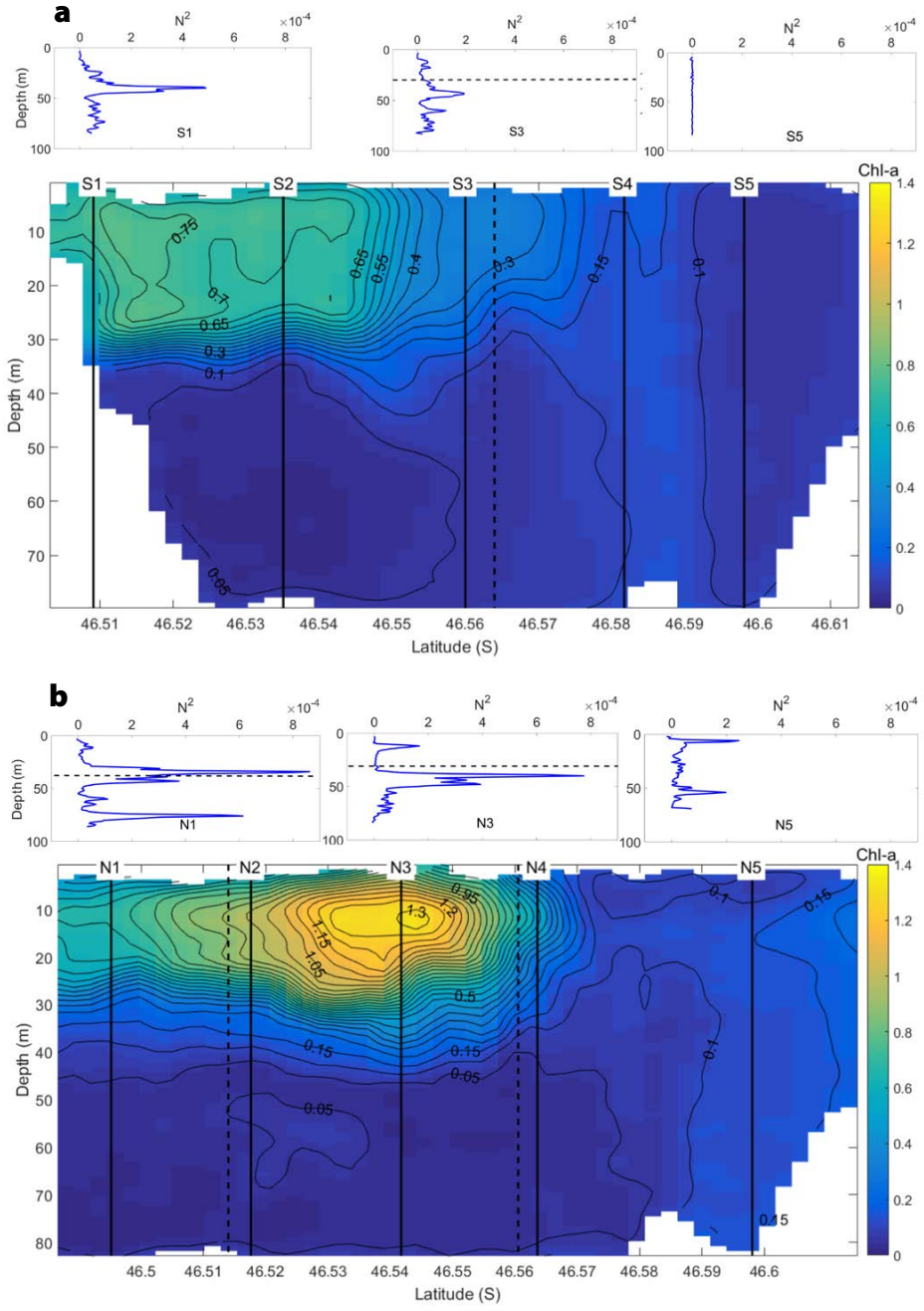

FIGURE 3. (top row) Brunt-Väisälä frequency (N^2, s^{-2}) for the CTD-rosette-sampled stations and euphotic depth Z_{eu} (black dotted line). Chl-*a* (mg m^{-3}) concentrations in the southern ROTV transects for (a) spring tide (S stations) and (b) neap tide (N stations).

The Effect of Eddies on Nutrient Distribution

The Pingree (1979) model (Equation 1 in Box 1, and Table 1) was used to estimate nutrient fluxes (Q_e, mg m^{-1} s^{-1}) due to mesoscale variability resulting from baroclinic instabilities (Mann and Lazier, 1996). In frontal zones, these features appear at the surface as meanders (Figure 2b). Here, the Pingree model results for the SJG are compared with two sites: Ushant front and Georges Bank, previously studied by Pingree (1979) and Loder and Platt (1985).

In the SJG frontal area, the pycnocline is twice as deep as it is at the Ushant front (in the Iroise Sea off the coast of western Brittany, France) and at Georges Bank, but the density differences across the fronts are smaller, so that the horizontal density gradient at the surface is less sharp here. Results show that the largest differences in nutrient concentrations between the stratified and the mixed sides (ΔC) occurred during neap tide (Table 1), when nutrient fluxes (Q_e) were higher (Q_e = 0.13 mg m^{-1} s^{-1}) than at the Ushant front (Q_e = 0.08 mg m^{-1} s^{-1}), Georges

BOX 1. Pingree (1979) Model Description

The Pingree (1979) model estimates nutrient flux (Q_e). ΔC and $\Delta\rho$ are the differences in nutrient concentration and density, respectively, across the front; γ is a constant (equal to 0.0055); g is the gravitational acceleration; ρ_0 is standard seawater density (1,026 kg m^{-3}), and D is pycnocline depth (m).

$$Q_e = \gamma \left(g \cdot \Delta\rho \frac{D}{\rho_0} \right)^{1/2} D \cdot \Delta C \quad (1)$$

This model was applied to spring and neap tide conditions separately, where ΔC and $\Delta\rho$ have different values, considering that the advection time of a water parcel due to eddies is determined by the inertial period, or 1/f, of an eddy, where f is the frequency (Pingree et al., 1979), which is smaller than the spring-neap tide time period.

bank (Q_e = 0.06 mg m^{-1} s^{-1}), and the SJG during spring tide (Q_e = 0.031 mg m^{-1} s^{-1}).

In contrast with the Q_e fluxes, during neap tide, stratified stations N1 and N3 present the lowest discrete nutrient concentrations in the upper mixed layer (Figure 4a), and also the lowest N:P ratio at the Chl-*a* maximum (<2; Figure 4b). Phosphate (P) concentrations are ~1 µM at all stations. Silicate (Si) concentrations are <2 µM, with the exception of S3, which reaches 6 µM. Nitrates (inorganic nitrate + nitrite: N) are <1 µM at N1 and N3, but >3 µM at other stations, with a maximum value at S1.

Regarding Redfield's balanced C:N ratio, Figure 5a shows values generally <7 at all stations, indicative of high-quality organic matter that decreases as stratification increases (larger N^2) and is maximal (C:N ~7) at stations S5 and S3, where stratification is weak. Stations N3 and N1, located where stratification is strong, display the minimal C:N ratio (~2–4).

Cell Carbon Content

Figure 5b plots particulate organic carbon (POC) for autotroph + heterotroph biomass (AHB). The *y* intercept of the regression shows that POC reaches 94 mg C m^{-3} when the contribution of living biomass is zero, probably provided by detritus (dead matter) or fecal pellets.

In terms of biomass, most of the autotrophic organisms belong to the nanophytoplankton size class (2–20 µm) at almost all stations. However, at station S1, microplanktonic (>20 µm) autotrophic dinoflagellates register the highest carbon contribution. At station S3, as mentioned above, micro-diatoms contribute to total biomass (Figure 6a).

Stations N1 and N3 exhibit the highest phytoplankton carbon values, in line with the highest Chl-*a* values obtained from ROTV transects, where nanophytoplankton, picophytoplankton, and cyanobacteria were the most important groups. At the well-mixed stations, N5 and S5, minimal phytoplankton biomass concentrations were observed.

TABLE 1. Pingree (1979) model comparing three tidal frontal zones.

	Ushant Front	Georges Bank	SJG (Spring Tide)	SJG (Neap Tide)
Depth (m)	20	20	40	40
$\Delta\rho/\rho_0$	6.7×10^{-4}	10^{-3}	5.2×10^{-5}	1.06×10^{-4}
ΔC (mg m^{-3})	2	0.67	1.03	3.05
γ	0.0055	0.01	0.0055	0.0055
Q_e (mg m^{-1} s^{-1})	0.08	0.06	0.031	0.13

D = depth. ρ = density. C = nutrient concentration. γ = constant. Q_e = nutrient flux.

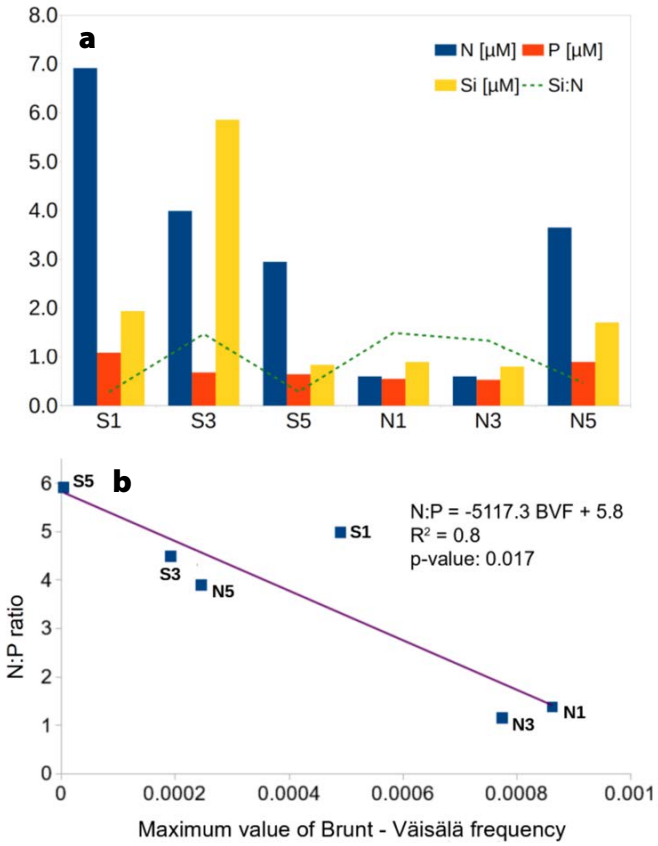

FIGURE 4. (a) Nutrient concentrations in the upper mixed layer (mg m^{-3}). Blue, orange, and yellow bars correspond to nitrates, phosphates, and silicates, respectively. The green dashed line shows the Si:N ratio. (b) Linear regression of the N:P ratio as a function of the maximum value of N^2 at each station.

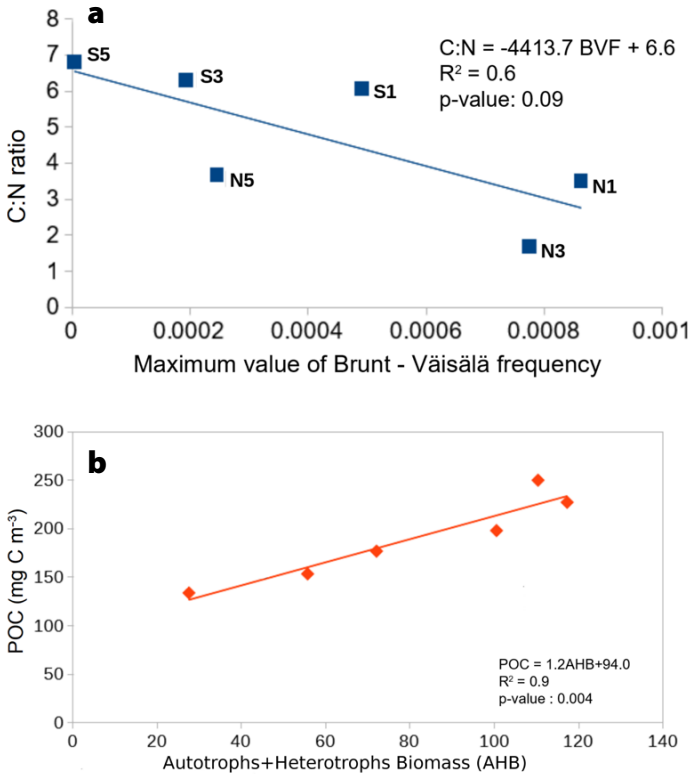

FIGURE 5. (a) C:N ratio as a function of the maximum N^2 at each station. (b) Linear regression of particular organic carbon (POC) vs. autotrophic + heterotrophic biomass (AHB) in mg C m^{-3}. Regression statistics were evaluated with RStudio (3.2.3; R Core Team, 2015).

Bacteria were the most important contributors to total heterotrophic biomass during neap tide, whereas heterotrophic ciliates and heterotrophic dinoflagellates also reached high values during spring tide (Figure 6b) in the stratified side of the front (stations S1 and S3). The stations with minimal heterotrophic biomass, S5 and N5, coincided with minimal Chl-*a* concentrations and well-mixed water conditions.

To understand how environmental conditions in the frontal zone (i.e., mixed-stratified water column, nutrient availability, euphotic depth) affect the physiological state of the autotrophic assemblages, we studied two key photosynthetic parameters at two depths: at the surface and at the Chl-*a* maximum depth (Figure 6c,d). With the exception of station S1, cells showed photoinhibition at the surface and were in better physiological condition at the Chl-*a* maximum depth (Figure 6c). A similar pattern to that of ***F***v/***F***m was observed for the parameter ***p*** but better responses (highest ***p***) were found at stations N1 and N3 (Figure 6d).

In the well-mixed stations S5 and N5, where cell abundances and biomass were the lowest, the physiological state of cells was similar to that of the other stations.

Comparing the *p*-value between spring and neap tide at the Chl-*a* maximum depth, it can be noted that photosynthetic efficiency is lower during spring tide than during neap tide.

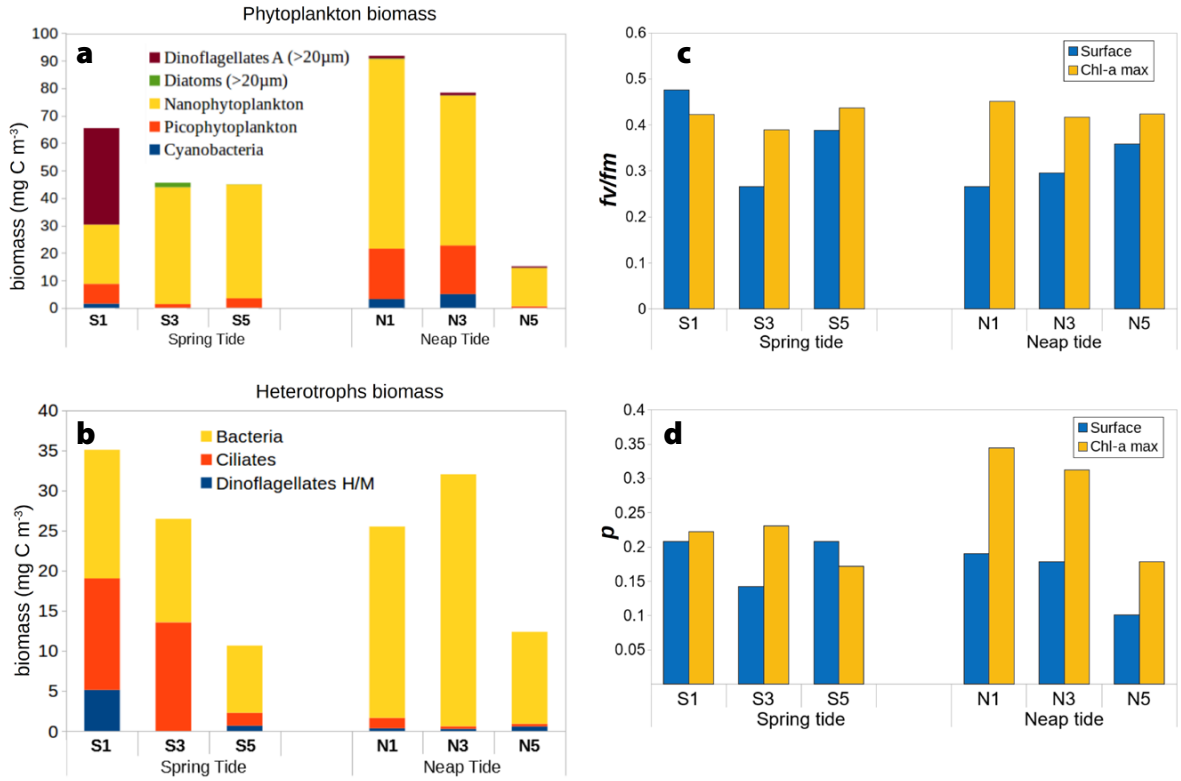

FIGURE 6. (a) Biomass (mg C m^{-3}) of main phytoplankton groups and (b) biomass of main heterotrophic groups. (c) ***F***v/***F***m parameter. (d) *p*-value. For (c) and (d), the blue bars are the photosynthetic quantum yield of phytoplankton cells at the surface and the yellow bars are Chl-*a* at maximum depth.

DISCUSSION

Baroclinic instabilities are mesoscale features that are generated by the potential energy difference across the front and that produce eddy-like structures (Mann and Lazier, 1996). It is well known that frontal boundaries are not stable and may be altered by the presence of eddies (Pingree, 1979). These mesoscale features can remain for a few days while influencing the exchange of nutrients and organisms across the frontal region (Pingree et al., 1979).

The calculated Z_{eu} reached 30–40 m, which is of the same order as that calculated by Carreto et al. (2016) for the Patagonian shelf break. The coastal area presents an even shallower Z_{eu} as a consequence of terrestrial dust and resuspension of particles from the bottom. The ratio between the upper mixed layer and Z_{eu} provides an indication of the conditions for growth and biomass accumulation in surface waters. In this case, Z_{eu} is similar to the pycnocline (black dotted line, N^2 profiles, Figure 3)

Stations located in stratified waters during neap tide presented maximum Chl-*a* concentrations, but these values were lower than previously reported for the southern SJG frontal zone during summer (2–2.3 mg Chl-*a* m^{-3}; Cucchi-Colleoni and Carreto, 2001)

The minimal nutrient fluxes estimated by the Pingree (1979) model for spring tide are consistent with the density distribution during this period (see Figure 1a,b) when there is no evidence of double frontal expression or eddies.

In marine coastal waters, nitrogen is the main limiting nutrient for phytoplankton productivity (Townsend and Pettigrew, 1997). No previous records exist for nitrate concentrations during summer in the SJG. Surface concentrations during spring are ~0.5–2 µM (Akselman, 1996). Furthermore, Si concentrations are <2 µM (and KSi limitation values vary between 3.9 µM and 5.0 µM; Sarthou et al., 2005). Therefore, we conclude that there is also an Si-limiting condition at all stations, with the exception of station S3 (5.9 µM Si). At S3, we observed that diatoms made only a small contribution to total phytoplankton biomass. Stations N1 and N3 present co-limitation by Si and N.

The low Si levels and the simultaneous absence of diatoms sampled at the other stations could be a consequence of the early consumption of Si by diatoms (as at stations S1 and S5) and grazing by micro- and mesozooplankton. During neap tide, stratified stations present an Si and N co-limitation, indicating that the timing of our study coincided with post-bloom conditions, and that primary producers were likely under intense grazing pressure.

It is noteworthy that the stations where nitrogen availability was minimal (N1 and N3, Figure 4a) are the most stratified ones, where the pycnocline separates deeper, nutrient-rich waters from the upper, nutrient-poor layer. These conditions are also evident when plotting the N:P ratio of the Chl-*a* maximum against water column stratification (Figure 4b). Considering that phytoplankton cells are able to incorporate nitrate at external concentrations as low as 0.2–0.3 µM (Sarthou et al., 2005), nitrate concentrations at stations N1 and N3 apparently were not limiting phytoplankton growth. However, a decrease of the atomic N:P ratio, which is ~16 under nutrient balanced conditions (Redfield, 1934), is observed at all stations plotted in Figure 4b, representing N-limiting conditions for autotrophic productivity (Geider and La Roche, 2002).

Although the model used here suggests high horizontal nutrient fluxes (Table 1, Box 1), absolute concentrations are not high, suggesting nutrients were either horizontally advected away from the sampled zone or rapidly consumed by phytoplankton. Stations S5 and S3 were the most vertically mixed, as shown by N^2. Station S5 was the only station where N:P was close to 6 at the Chl-*a* maximum, which could result from intense mixing during the entire fortnightly cycle, as shown in other areas (Geider and LaRoche, 2002). By contrast, while Pingree's model showed the smallest nutrient flux during spring tide (Table 1), the stations we sampled during spring tide (S1, S3, and S5, Figure 4a) presented the highest nutrient concentrations. This could be due to an accumulation effect, with two possible scenarios that could be related to the planktonic food web:

1. Minimal uptake of inorganic nutrients. This could have happened if: (a) photosynthetic organisms were under high grazing pressure but were actively producing high-quality organic matter (i.e., low C:N ratios), that is, energy was rapidly transferred to the upper levels of the food web, or (b) phytoplankton were in poor condition, and physiological parameters such as the ratio of variable to maximum fluorescence, $\boldsymbol{F}v/\boldsymbol{F}m$, and the connectivity parameter $\boldsymbol{p}$ had relatively low values.
2. Physical accumulation effect. If the energy transfer between the different food web levels were slow, bacteria would accumulate and productivity would be enhanced by recycling in the microbial loop. Consequently, organic matter degradation would be very important and the C:N ratio could reach higher values (over 7; Caron et al., 1995).

According to the nutrient models, stations N1 and N3 received strong nutrient fluxes. Because their concentrations were low, we hypothesize that inorganic nutrients at these stations were being quickly assimilated and transformed into new organic matter. Even if station S1 exhibited high nutrient availability (Figure 4a), there was less autotrophic biomass accumulation. These results suggest high grazing pressure, considering the high biomass of ciliates and heterotrophic dinoflagellates, which is consistent with the first of the above-hypothesized scenarios. Consequently, low phytoplankton accumulation could be explained by an intense production-grazing coupling.

Regarding phytoplankton biomass, it is noteworthy that station S3, the closest to the frontal position during spring tide, received a micro-diatom contribution

to total biomass (Figure 6a), and as theory predicts, diatoms tend to dominate in nutrient-rich, turbulent waters (Glibert, 2016).

Phytoplankton organic matter is usually high in protein, carbohydrates, and lipids (Copin-Montegut and Copin-Montegut, 1983). Redfield's balanced 6.6 C:N ratio can indeed reach values from 3.8 to 12.5 (Geider and La Roche, 2002), although values between 8 and >15 are common in deep waters, while in the surface layer, the C:N ratio may range from 5 to 8 (Copin-Montegut and Copin-Montegut, 1983). Low C:N ratios are indicative of high-quality food for consumers, and an increase in this ratio is related to detritus or heterotrophic organism increases (Townsend and Thomas 2002), suggesting more rapid utilization of proteins than carbohydrates (Copin-Montegut and Copin-Montegut, 1983). The C:N ratio (Figure 5a) shows values generally <7 at all stations, indicative of high-quality organic matter that decreases as stratification increases (larger N^2). When C and N are actively incorporated into nucleic acids, amino acids, or proteins, cells' C:N ratios can vary from 2.6 to 3.8 (Geider and La Roche, 2002). Weak stratification conditions displayed the highest C:N ratio (~7), probably influenced by degraded organic matter resuspended from the bottom by vertical mixing. Stations located where stratification was strong display the minimal C:N ratio, around 2–4, indicating high-quality organic matter. These C:N ratio results support the first proposed scenario.

The regression of the AHB vs POC plot (Figure 5b) indicates that more than 60% of the POC is composed of particulate organic matter made up of detritus and fecal pellets (Valérie Massé-Beaulne, Université du Québec à Rimouski, *pers. comm.*, 2018).

Considering that the smallest cells, such as picoeukaryotes, have an ***F***v/***F***m signature between 0.3 and 0.4 and that the signature for cyanobacteria ranges between 0.1 and 0.4 (Suggett et al., 2009), we can infer that cells were photosynthetically active in the environmental conditions of the frontal zone. However, the lowest *p*-values were found at Chl-*a* maximum depth during spring tide.

We hypothesize that although cells are being transported from the surface to the bottom, they are able to adapt their photosynthetic apparatus to the average light intensity of the water column (Moore et al., 2006). Moreover, nutrient availability does not seem to affect the photosynthetic parameters studied.

The minimal uptake of inorganic nutrients during spring tide seems to be a result of the combined factors proposed in the first scenario discussed above, where the relatively poorer condition of phytoplankton (at Chl-*a* maximum depth) and strong grazing pressure are related to the production of new organic matter with high nutritional quality that is available to higher trophic levels in the marine food web.

CONCLUSIONS

Tidal fronts act as boundaries, usually separating deep stratified waters from well-mixed shallow waters (Loder and Platt, 1985). However, a relatively shallow zone in the southern SJG surrounded by deeper waters (Glembocki et al., 2015) extends the frontal zone offshore. Here, variability in mesoscale activity rather than in tidal energy control the variability in the front's position. Stratification (as N^2) allowed us to separate stations S1, N1, N3 ($N^2 \geq 4 \times 10^{-4}$ s^{-2}) from stations S3, S5, and N5 ($N^2 \leq 2 \times 10^{-4}$ s^{-2}). Inorganic nitrogen availability was high at station S3 at the frontal interface, but the quality of the organic matter was lower than at the other stations. The main phytoplankton groups, in terms of biomass, were nanoeukaryotes and microplanktonic diatoms, and the main heterotrophic groups were bacteria and ciliates. All stations presented an N:P ratio <16 suggesting N-limiting conditions, although not to a critical level, and some Si limitation in several stations.

Because the calculated horizontal nutrient flux is weak during spring tide, we expected quick uptake by autotrophic organisms, and, consequently, low inorganic nutrient concentrations and high phytoplankton cell densities (i.e., low C:N ratios). In the whole area, the high cyanobacteria biomass probably provides relatively high amounts of nitrogenous compounds, resulting in C:N ratios ~7 during summer. However, station S1 presented high inorganic N concentration above the pycnocline, and plankton assemblages there included large microphytoplankton cells such as autotrophic dinoflagellates, which have a slow growth rate and long life cycles, and are able to swim in order to search for their optimal growth conditions (Glibert, 2016). Nevertheless, this community was probably under high grazing pressure by mesozooplankton. Giménez et al., (2018, in this issue) described high copepodit and *Ctenocalanus vanus* abundances and high young euphausiid stage (including *Euphausia vallentini*) and *Ctenocalanus vanus* biomass in the frontal area. The dynamics of this food web results in large amounts of detritus that mainly consist of large particles such as fecal pellets and macroaggregates.

During neap tide, the stratified stations N1 and N3 displayed high nutrient fluxes, although nutrient concentrations were low. The assimilation of nutrients by autotrophic organisms is supported by the presence of high cell densities and autotrophic and heterotrophic biomass. This microbial community was very different from that developed during spring tide, and was characterized by small photosynthetic cells and high bacterial density and biomass. These organisms have short life cycles and high growth rates and grow on regenerated production, typical of microbial loops (Glibert, 2016). This agrees with the observed N:P ratio, which is ~0 when recycled production fuels primary production (Townsend and Thomas, 2002). The *p*-value was maximum at stations N1 and N3, around 0.3 and 0.4. Considering that the dominating cyanobacteria in the area usually have a signature in natural environments

between 0.1 and 0.4 (Suggett et al., 2009), we can conclude that optimal light and nutrient conditions for cyanobacteria growth characterized all stations.

To synthesize some of our findings, we built a conceptual model to show the dynamics of nutrients and microbial groups during both tidal periods on the stratified side of the front (Figure 7). During spring tide (Figure 7a), large cells (>20 µm) mainly supply the autotrophic biomass (Phy). However, the largest phytoplankton biomass was found during neap tide (Figure 7b), when small cells (<20 µm) are the most important in terms of biomass. Heterotrophic biomass was divided into bacteria (B) and eukaryotic heterotrophs (H), such as dinoflagellates and ciliates. During spring tide, H contributes the most to the heterotrophic biomass, while during neap tide, B is more relevant than H. The relative low C:N ratio during neap tide is representative of the better quality organic matter during that period, highlighting the importance of nano- and picophytoplankton in marine primary production. Overall, our results provide evidence that there are strong links between physical, chemical, and biological patterns and processes in tidal fronts, emphasizing the importance of integrated mesoscale studies in coastal areas.

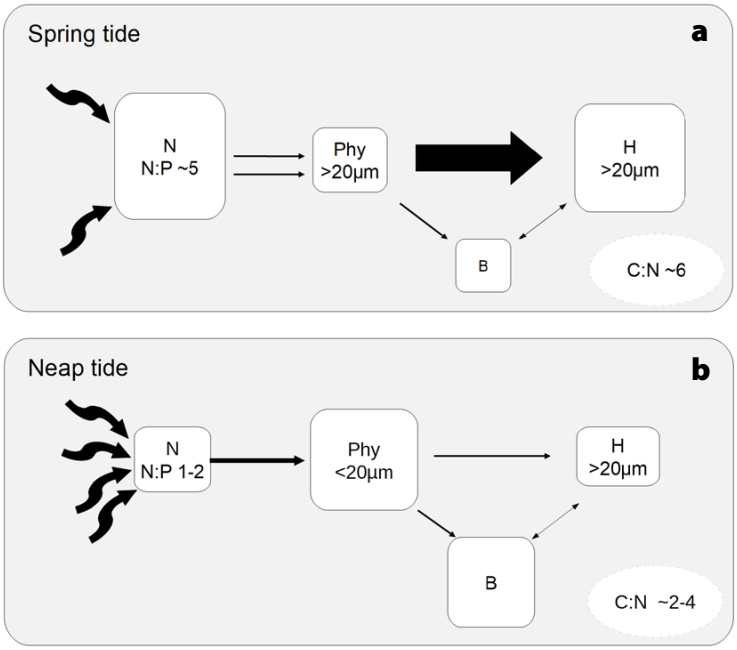

FIGURE 7. Conceptual model showing the dynamics of nutrients and microbial groups during (a) spring tide and (b) neap tide on the stratified side of the front. Arrows represent the energy transfer between compartments (squares)—the stronger the interaction, the thicker the arrow. N:P = Nitrate to phosphate ratio. Phy = Phytoplankton. H = Heterotrophs. B = Bacteria. C:N = Carbon to nitrate ratio. The width of the arrows indicates the strength of the interaction.

SUPPLEMENTARY MATERIALS

Supplementary materials are available online at https://doi.org/10.5670/oceanog.2018.412.

REFERENCES

Acha, E.M., A. Piola, O. Iribarne, and H. Mianzan. 2015. *Ecological Processes at Marine Fronts: Oases in the Ocean*. Springer International Publishing, 68 pp.

Akselman, R. 1996. *Estudios ecológicos en el Golfo San Jorge y adyacencias (Atlántico Sudoccidental): Distribución, abundancia y variación estacional del fitoplancton en relación a factores Físico-químicos y la dinámica hidrológica*. PhD dissertation, Facultad de Ciencias Exactas y Naturales, Universidad de Buenos Aires.

Barros, V.R. 1983. *Atlas del potencial eólico de la Patagonia*. Biblioteca Centro Nacional Patagonico Contribución 69, Argentina, 171 pp.

Belzile, C., and M. Gosselin. 2015. Free-living stage of the unicellular algae *Coccomyxa* sp. parasite of the blue mussel (*Mytilus edulis*): Low-light adaptation, capacity for growth at a very wide salinity range and tolerance to low pH. *Journal of Invertebrate Pathology* 132:201–207, https://doi.org/10.1016/j.jip.2015.10.006.

Bertilsson, S., O. Berglund, D.M. Karl, and S.W. Chisholm. 2003. Elemental composition of marine *Prochlorococcus* and *Synechococcus*: Implications for the ecological stoichiometry of the sea. *Limnology and Oceanography* 48(5):1,721–1,731, https://doi.org/10.4319/lo.2003.48.5.1721.

Borsheim, K.Y., and G. Bratbak. 1987. Cell volume to cell carbon conversion factors for a bacterivorous Monas sp. enriched from seawater. *Marine Ecology Progress Series* 36:171–175, https://doi.org/10.3354/meps036171.

Caron, D.A., H.G. Dam, P. Kremer, E.J. Lessard, L.P. Madin, T.C. Malone, J.M. Napp, E.R. Peele, M.R. Roman, and M.J. Youngbluth. 1995. The contribution of microorganisms to particulate carbon and nitrogen in surface waters of the Sargasso Sea near Bermuda. *Deep Sea Research Part I* 42(6):943–972, https://doi.org/10.1016/0967-0637(95)00027-4.

Carreto, J. I., N.G. Montoya, M.O. Carignan, R. Akselman, E.M. Acha, and C. Derisio. 2016. Environmental and biological factors controlling the spring phytoplankton bloom at the Patagonian shelf-break front: Degraded fucoxanthin pigments and the importance of microzooplankton grazing. *Progress in Oceanography* 146:1–21, https://doi.org/10.1016/j.pocean.2016.05.002.

Copin-Montegut, C., and G. Copin-Montegut. 1983. Stoichiometry of carbon, nitrogen, and phosphorus in marine particulate matter. *Deep Sea Research Part A* 30(1):31–46, https://doi.org/10.1016/0198-0149(83)90031-6.

Cucchi-Colleoni, D.A., and J.I. Carreto. 2001. *Variación estacional de la biomasa fitoplanctónica en el Golfo San Jorge. Resultados de las Campañas de Investigación OB-01/00, OB-03/00, OB-07/00, OB-10/00 y OB-12/00*. Instituto Nacional de Desarrollo Pesquero, Argentina, 30 pp.

Fernández, M., J.I. Carreto, J. Mora, and A. Roux. 2005. Physico-chemical characterization of the benthic environment of the Golfo San Jorge, Argentina. *Journal of the Marine Biological Association of the United Kingdom* 85(6):1,317–1,328, https://doi.org/10.1017/S002531540501249X.

Fernández, M., J. Mora, A. Roux, D.A. Cucchi-Colleoni, and J.C. Gasparoni. 2008. New contribution on spatial and seasonal variability of environmental conditions of the Golfo San Jorge benthic system, Argentina. *Journal of the Marine Biological Association of the United Kingdom* 88(2):227–236, https://doi.org/10.1017/S0025315408000465.

Franks, P.J. 1992. Phytoplankton blooms at fronts: Patterns, scales, and physical forcing mechanisms. *Reviews in Aquatic Sciences* 6(2):121–137.

Geider, R., and J. LaRoche. 2002. Redfield revisited: Variability of C:N:P in marine microalgae and its biochemical basis. *European Journal of Phycology* 37(1):1–17, https://doi.org/10.1017/S0967026201003456.

Giménez, E.M., G. Winkler, M. Hoffmeyer, and G.A. Ferreyra. 2018. Composition, spatial distribution, and trophic structure of the zooplankton community in San Jorge Gulf, southwestern Atlantic Ocean. *Oceanography* 31(4):154–163, https://doi.org/10.5670/oceanog.2018.418.

Glembocki, N.G., G.N. Williams, M.E. Góngora, D.A. Gagliardini, and J.M.L. Orensanz. 2015. Synoptic oceanography of San Jorge Gulf (Argentina): A template for Patagonian red shrimp (*Pleoticus muelleri*) spatial dynamics. *Journal of Sea Research* 95:22–35, https://doi.org/10.1016/j.seares.2014.10.011.

Glibert, P.M. 2016. Margalef revisited: A new phytoplankton mandala incorporating twelve dimensions, including nutritional physiology. *Harmful Algae* 55:25–30, https://doi.org/10.1016/j.hal.2016.01.008.

Glorioso, P.D., and R.A. Flather. 1995. A barotropic model of the currents off SE South America. *Journal of Geophysical Research* 100(95):427–440, https://doi.org/10.1029/95JC00942.

Hillebrand, H., C.D. Durselen, D. Kirschtel, U. Pollingher, and T. Zohary. 1999. Biovolume calculation for pelagic and benthic microalgae. *Journal of Phycology* 35:403–424, https://doi.org/10.1046/j.1529-8817.1999.3520403.x.

Kirk, J.T.O. 1994. *Light and Photosynthesis in Aquatic Systems*, 2nd ed. Cambridge University Press. Cambridge, UK, 509 p.

Landeira, J.M., B. Ferron, M. Lunven, P. Morin, L. Marie, and M. Sourisseau. 2014. Biophysical interactions control the size and abundance of large phytoplankton chains at the Ushant tidal front. *PLoS ONE* 9(2):1–14, https://doi.org/10.1371/journal.pone.0090507.

Loder, J.W., and T. Platt. 1985. Physical controls on phytoplankton production at tidal fronts. *Proceedings of the Nineteenth European Marine Biology Symposium*: *Plymouth*. September 16–21, 1984, Devon, UK.

Louge, E.B., R. Reta, B.A. Santos, and D.R. Hernández. 2004. *Variaciones interanuales (1995–2000) de la temperatura y la salinidad registradas en los meses de enero en el Golfo San Jorge y aguas adyacentes (43°S–47°S)*. Instituto Nacional de Desarrollo Pesquero, Revista de Investigación y Desarrollo Pesquero, Contribución 16, 15 pp.

Mann, K.H., and J.R.N. Lazier. 1996. *Dynamics of Marine Ecosystems: Biological-Physical Interactions in the Oceans*. Blackwell Science Publications, Cambridge, 394 pp.

Margalef, R. 1978. Life-forms of phytoplankton as survival alternatives in an unstable environment. *Oceanologica* 1(4):337–341, http://doi.org/10.1590/S0102-09352000000400008.

Maxwell, K., and G.N Johnson. 2000. Chlorophyll fluorescence: A practical guide. *Journal of Experimental Botany* 51(345):659–668, https://doi.org/10.1093/jexbot/51.345.659.

McDougall, T.J., and P.M. Barker. 2011. Getting started with TEOS-10 and the Gibbs Seawater (GSW) oceanographic toolbox. *SCOR/IAPSO WG* 127:1–28.

Menden-Deuer, S., and E.J. Lessard. 2000. Carbon to volume relationships for dinoflagellates, diatoms, and other protist plankton. *Limnology and Oceanography* 45(3):569–579, https://doi.org/10.4319/lo.2000.45.3.0569.

Moore, C.M., D.J. Suggett, A.E. Hickman, Y.N. Kim, J.F. Tweddle, J. Sharples, R.J. Geider, and P.M. Holligan. 2006. Phytoplankton photoacclimation and photoadaptation in response to environmental gradients in a shelf sea. *Limnology and Oceanography* 51(2):936–949, https://doi.org/10.4319/lo.2006.51.2.0936.

Olenina, I., S. Hajdu, L. Edler, A. Andersson, N. Wasmund, S. Busch, J. Göbel, S. Gromisz, S. Huseby, M. Huttunen, and others. 2006. *Biovolumes and Size-Classes of Phytoplankton in the Baltic Sea*. Helsinki Commission - Baltic Sea Environment Proceedings No. 106, 144 pp.

Palma, E.D., R.P. Matano, and A.R. Piola. 2004. A numerical study of the Southwestern Atlantic Shelf circulation: Barotropic response to tidal and wind forcing. *Journal of Geophysical Research* 109(8):1–17, https://doi.org/10.1029/2004JC002315.

Pingree, R.D. 1979. Baroclinic eddies bordering the Celtic Sea in late summer. *Journal of the Marine Biological Association of the United Kingdom* 59(3):689–698, https://doi.org/10.1017/s0025315400045677.

Pingree, R.D., P.M. Holligan, and G.T. Mardell. 1978. The effects of vertical stability on phytoplankton distributions in the summer on the northwest European shelf. *Deep Sea Research* 25(11):1,011–1,016, https://doi.org/10.1016/0146-6291(78)90584-2.

Pingree, R.D., P.M. Holligan, and G.T. Mardell. 1979. Phytoplankton growth and cyclonic eddies. *Nature* 278(5701):245–247, https://doi.org/10.1038/278245a0.

R Core Team. 2015. R: A language and environment for statistical computing. R Foundation for Statistical Computing, Vienna, Austria, https://www.R-project.org.

Redfield, A.C. 1934. On the proportions of organic derivatives in sea water and their relation to the composition of plankton. Pp. 176–192 in *James Johnstone Memorial Volume*. R.J. Daniel, ed., University of Liverpool.

Rivas, A.L. 1997. Current-meter observations in the Argentine continental shelf. *Continental Shelf Research* 17(4):391–406.

Rivas, A.L. 2006. Quantitative estimation of the influence of surface thermal fronts over chlorophyll concentration at the Patagonian shelf. *Journal of Marine Systems* 63(3–4):183–190, https://doi.org/10.1016/j.jmarsys.2006.07.002.

Sarthou, G., K.R. Timmermans, S. Blain, and P. Tréguer. 2005. Growth, physiology and fate of diatoms in the ocean: A review. *Journal of Sea Research* 53:25–42, https://doi.org/10.1016/j.seares.2004.01.007.

Skalar Analytical BV. 2005. The SANplus segmented flow analyser: Soil and plant analysis. Skalar Analytical BV, Netherlands, software.

Simpson, J.H., and J.R. Hunter. 1974. Fronts in the Irish Sea. *Nature* 250(5465):404–406, https://doi.org/10.1038/250404a0.

Suggett, D.J., C.M. Moore, A.E. Hickman, and R.J. Geider. 2009. Interpretation of fast repetition rate (FRR) fluorescence: Signatures of phytoplankton community structure versus physiological state. *Marine Ecology Progress Series* 376:1–19, https://doi.org/10.3354/meps07830.

Strickland, J.D.H., and T.R. Parsons. 1972. *A Practical Handbook of Seawater Analysis*. Fisheries Research Board of Canada, Ottawa, 310 pp.

Tarran, G.A., J.L. Heywood, and M.V. Zubkov. 2006. Latitudinal changes in the standing stocks of nano- and picoeukaryotic phytoplankton in the Atlantic Ocean. *Deep Sea Research Part II* 53:1,516–1,529, https://doi.org/10.1016/j.dsr2.2006.05.004.

Tonini, M., E. Palma, and A. Rivas. 2006. Modelo de alta resolución de los golfos patagónicos. *Asociación Argentina de Mecánica Computacional* 15:1,441–1,460, https://doi.org/10.1017/CBO9781107415324.004.

Townsend, D.W., and N.R. Pettigrew. 1997. Nitrogen limitation of secondary production on Georges Bank. *Journal of Plankton Research* 19(2):221–235, https://doi.org/10.1093/plankt/19.2.221.

Townsend, D.W., and M. Thomas. 2002. Springtime nutrient and phytoplankton dynamics on Georges Bank. *Marine Ecology Progress Series* 228:57–74, https://doi.org/10.3354/meps228057.

Utermöhl, H. 1958. Zur Vervollkommnung der quantitativen Phytoplankton-Methodik: Mit 1 Tabelle und 15 abbildungen im Text und auf 1 Tafel. *Internationale Vereinigung für theoretische und angewandte Limnologie: Mitteilungen*, *9*(1):1–38.

Zubkov, M.V., M.A. Sleigh, and P.H. Burkill. 2000. Assaying picoplankton distribution by flow cytometry of underway samples collected along a meridional transect across the Atlantic Ocean. *Aquatic Microbial Ecology* 21(1):13–20, https://doi.org/10.3354/ame021013.

ACKNOWLEDGMENTS

This work was funded by the PROMESse project (http://coriolis.uqar.ca/), a partnership between the Ministerio de Ciencia, Teconología e Innovación Productiva de la República Argentina (MINCyT), the Province of Chubut (Secretaría de Medio Ambiente y Desarrollo Sustentable de la Nación), the Consejo Nacional de Investigaciones Científicas y Técnicas (CONICET), and the Université du Québec à Rimouski/Institut des sciences de la mer de Rimouski (UQAR-ISMER) in collaboration with Bec.Ar program, and Québec-Océan. Also, we wish to thank the *Coriolis II* crew and Captain Emmanuel Sevor.

AUTHORS

Ximena Flores-Melo (ximenafloresmelo@gmail.com) completed her master's degree at Institut des Sciences de la Mer (ISMER), Université du Québec à Rimouski, Québec, Canada, and is currently at Centro Austral de Investigaciones Científicas (CADIC)-Consejo Nacional de Investigaciones Científicas y Técnicas (CONICET), Ushuaia, Tierra del Fuego, Argentina. **Irene R. Schloss** is Researcher, Instituto Antártico Argentino, CADIC, Tierra del Fuego, Argentina; Associate Professor, ISMER, Université du Québec à Rimouski, Québec, Canada; and Professor, Universidad Nacional de Tierra del Fuego, Ushuaia, Tierra del Fuego, Argentina. **Cédric Chavanne** is Professor, ISMER, Université du Québec à Rimouski, Québec, Canada. **Gastón O. Almandoz** is a researcher at CONICET, División de Ficología, Facultad de Ciencias Naturales y Museo, Universidad Nacional de La Plata, La Plata, Argentina. **Maité Latorre** is a PhD candidate at the Centro para el Estudio de Sistemas Marinos, Centro Nacional Patagónico (CENPAT)-CONICET, Puerto Madryn, Chubut, Argentina. **Gustavo A. Ferreyra** is Head, CADIC-CONICET, Ushuaia, Tierra del Fuego, Argentina, and Associate Professor, ISMER, Université du Québec à Rimouski, Québec, Canada.

ARTICLE CITATION

Flores-Melo, X., I.R. Schloss, C. Chavanne, G.O. Almandoz, M. Latorre, and G.A. Ferreyra. 2018. Phytoplankton ecology during a spring-neap tidal cycle in the southern tidal front of San Jorge Gulf, Patagonia. *Oceanography* 31(4):70–80, https://doi.org/10.5670/oceanog.2018.412.